Electronic Supplementary Information (ESI)

Optically Transparent and Mechanically Tough Glass with Impact Resistance and Retardance Enabled by Covalent/Supramolecular Interactions

Changyong Cai[1], Guohong Yao[2], Yunfei Zhang[2], Shiguo Zhang[3], Fenfang Li[4], Zhijian Tan*[1]& Shengyi Dong*[2]

[1]Institute of Bast Fiber Crops, Chinese Academy of Agricultural Sciences, Hunan 410205, P. R. China

[2]College of Chemistry and Chemical Engineering, Hunan University, Hunan 410082, P. R. China

[3]College of Materials Science and Engineering, Hunan University, Changsha, 410082, P. R. China

[4]College of Chemistry and Chemical Engineering, Central South University, Hunan 410083, P. R. China

1. Materials and methods

1-Vinyl-3-ethylimidazolium tetrafluoroborate and 2-hydroxy-4'-(2-hydroxyethoxy)-2-methylpropiophenone were purchased from Shanghai Adamas Reagent Co., Ltd (China). Other commercially solvents and materials were used without purification. Solid-phase UV spectrum was recorded using a Shimadzu UV-3600i Plus (Japan). Powder X-ray diffraction (PXRD) spectra were collected on an Ultima IV (Japan). Thermogravimetric analysis (TGA) of samples were carried out using a Shimadzu TGA-50 (Japan), and the heating rate was 10 ºC min^{-1} from 30 to 800 ºC in nitrogen atmosphere. Differential Scanning Calorimeter (DSC) was carried out using a Mettler DSC3 (Switzerland), and the heating rate was 10 ºC min^{-1} from -80 to 300 ºC in nitrogen atmosphere. Scanning electron microscopy (SEM) images were collected on a Hitachi S4800 (Japan). Dynamic thermomechanical analyses (DMA) were performed on a DMA 8000-PerkinElmer (USA) using shear model. Small angle X-ray scattering (SAXS) was performed on an Anton Paar SAXSess (Austria). Nanoindentation were obtained by a Hysitron TI 950 (USA). Broadband dielectric measurements were performed through a Novocontrol Concept 80 system with Alpha impedance analyzer and Quatro Novocontrol Cryo-system temperature control (Germany). Frequency sweep mode was used with frequency range of 10^{-1} to 10^{6} Hz at each temperature from –40 to 140 °C with 10 °C interval by cell BDS 1308 (Novocontrol). Atomic force microscopy (AFM) measurements were carried out on a Bruker Dimension Icon AFM (Germany). Transmittance measurements were determined on a Ruike RK-6000 spectrometer (China). X-ray photoelectron spectroscopy (XPS) was carried out on a Thermo Kalpha (UK). Gel Permeation Chromatography (GPC) was carried out on a Waters GPC 1515 (USA) with dimethyl formamide as the eluent. The tensile strength and compressive data were tested by a universal testing machine (HT-10180-5, China). Impact resistance is measured by a digital impact tester XBL instrument (GB/T1043-2008). Shore hardness (HD) was tested by a digital hardness tester (China). Fluorescence spectroscopy and quantum yield were performed on an Edinburgh Instruments FLS980 (Britain). Density measurements were performed on XingYun XY-2CM (China). Laser engraving was performed on vodmicro-T6. Raman was carried out on a Horiba

LabRAM HR Evolution (Japan). pyrolysis-gas chromatography/mass spectrometry (Py-GC/MS) was carried out on GCMS-QP2020NX (Japan). TG-IR was carried out on a Thermo Fisher IS-50 (USA)

Full names of materials used in this study: polypropylene (PP), polyethylene (PE), polymethyl methacrylate (PMMA), polycarbonate (PC), acrylonitrile butadiene styrene copolymer (ABS), polypropylene (PP), polyethylene (PE), polyamide (PA), polyurethane (PU), polytetrafluoroethylene (PTFE), polyethylene terephthalate (PET), polystyrene (PS), polyvinyl chloride (PVC), and Polyformaldehyde (POM).

Preparation of AG

1-Vinyl-3-ethylimidazolium tetrafluoroborate was used to construct **AG** by irradiating at 405 nm curing light (UVGO, China) for 2 h, with 2-hydroxy-4'-(2-hydroxyethoxy)-2-methylpropiophenone as the photo-initiator.[1]

Broadband dielectric measurements and analyses

Broadband dielectric measurements were performed through a Novocontrol Concept 80 system with Alpha impedance analyzer and Quatro Novocontrol Cryo-system temperature control (Germany). Frequency sweep mode was used with frequency range of 10^{-1} to 10^{6} Hz at each temperature from –40 to 140 ºC with 10 ºC interval by cell BDS 1308 (Novocontrol). In this model, to extract quantitative information, the isothermal complex electric modulus spectra were deconvoluted according to the sum of two Havriliak-Negami functions.[2,3]

Temperature-dependent mechanical properties

Tensile, compressive, three-point bending, and impact experiments of **AG** were tested at different temperatures. **AG** was placed in a drying oven for 2 h at different temperatures before testing.

Creep recovery test

Creep recovery tests were performed at 25 and 80 °C upon a constant stress of 0.1 MPa.[4]

Flame retardant test

Flame retardant test was according previously reported methods.[5] The vertical burning test (UL-94) was carried out by a flame test chamber (FTT0082, UK) with ASTM D3801-10 standard. The size of **AG** is 120 × 13 × 4 mm. Six repeated experiments were conducted. The limiting oxygen index (LOI) was tested by a limiting oxygen index instrument (FTT0077, UK) with ASTM D2863-00 standard. The size of **AG** is 100 × 10 × 4 mm. Six repeated experiments were conducted. The flame retardancy of **AG** was tested by a cone calorimeter (FTT0007, UK) with ISO 5660–1 standard. The heat flux density is 50 kW m^{-2}. The size of **AG** is 80 × 80 × 3 mm. Two repeated experiments were conducted.

Mobile phone protection test of AG

1-Vinyl-3-ethylimidazolium tetrafluoroborate with 2-hydroxy-4'-(2-hydroxyethoxy)-2-methylpropiophenone was dropped onto the phone screen. Then, the liquid drop was paved and irradiated at 405 nm for 2 h. The phone screen with **AG** was smashed by a 250 g iron ball from a height of 0.5 m and recorded with a digital camera.

Theoretical simulation calculation

Quantum chemical calculations were carried out by using density functional theory (DFT) implemented in Gaussian 09 program. The structure optimization and single point energy were performed at B3LYP-GD3(BJ)/6-311G(d) level. The electrostatic potential and independent gradient model analysis were calculated by Multiwfn and Visual Molecular Dynamics software.[6,7] The binding energy E_B between the molecules was defined as:

$$E_B = E_{Total} - E_{Anion} - E_{Cation} \quad (3)$$

where E_{Total}, E_{Anion}, and E_{cation} are the energies of total, the anion, the cation of **AG**, respectively.

According to references, the GROMACS soft were used for Molecular Dynamics (MD) simulations.[8–10] The GAFF force field including the parameters of bonds, angles, dihedrals, and Lennard-Jones interactions for the all components were used. In this study, **AG** was simplified to consist of 50 repeating units. There are 40 polymer chains in the simulation system.

Refractive index and extinction coefficient of AG

AG was placed on the ellipsometer (J.A. Woollam RC2, USA) sample stage. The wavelength range is 200–2000 nm, with a step size of 0.5 nm for sample measurement; After obtaining the raw data, a model is established and fitted to obtain refractive index (n) and extinction coefficient (k). The models are new amorphous dispersion formulas (1–3).[11]

$$k(\omega) = \begin{cases} \sum_{j=1}^{N} \dfrac{f_j \cdot (\omega - \omega_g)}{(\omega - \omega_j)^2 + \Gamma_j^2}, & \text{for} \omega \geq \omega_g \\ 0, & \text{for} \omega < \omega_g \end{cases} \quad (1)$$

And for *n* there is:

$$n(\omega) = n_\infty + \sum_{j=1}^{N} \frac{B_j \cdot (\omega - \omega_j) + C_j}{(\omega - \omega_j)^2 + \Gamma_j^2} \quad (2)$$

where:

$$\begin{cases} B_f = \dfrac{f_f}{\Gamma_f} \cdot \left[\Gamma_f^2 - (\omega_f - \omega_g)^2\right] \\ C_f = 2 f_f \Gamma_f (\omega_f - \omega_g) \end{cases} \quad (3)$$

Were the subscripts *j = 1, 2… N* label the oscillator considered in the new amorphous dispersion formula. ω_g is the band gap energy, ω_j is approximately the photon energy at which *k(ω)* reaches maxima, fj is the oscillator strength, and Γ_j is the damping factor. The optical parameters to be fitted are: n_∞, ω_g, f_j, ω_j and Γ_j, *j = 1, 2, …, N*.

2. Gel Permeation Chromatography (GPC) of AG

Table S1. Molecular weight of **AG**.

	*M*p (Da)	*M*n (Da)	*M*w (Da)	*M*z (Da)	*M*z+1 (Da)	*M*v (Da)	PDI
AG	64711	48288	69501	93712	119615	66182	1.44

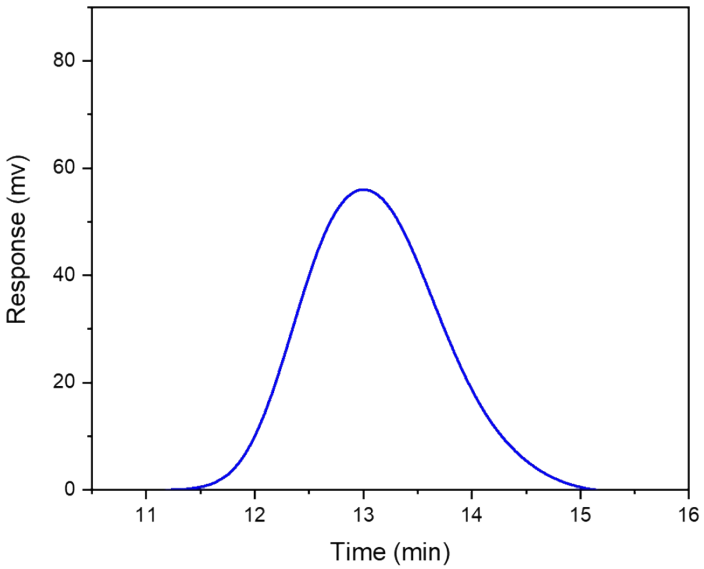

Figure S1. GPC spectrum of **AG**.

3. Morphological of AG

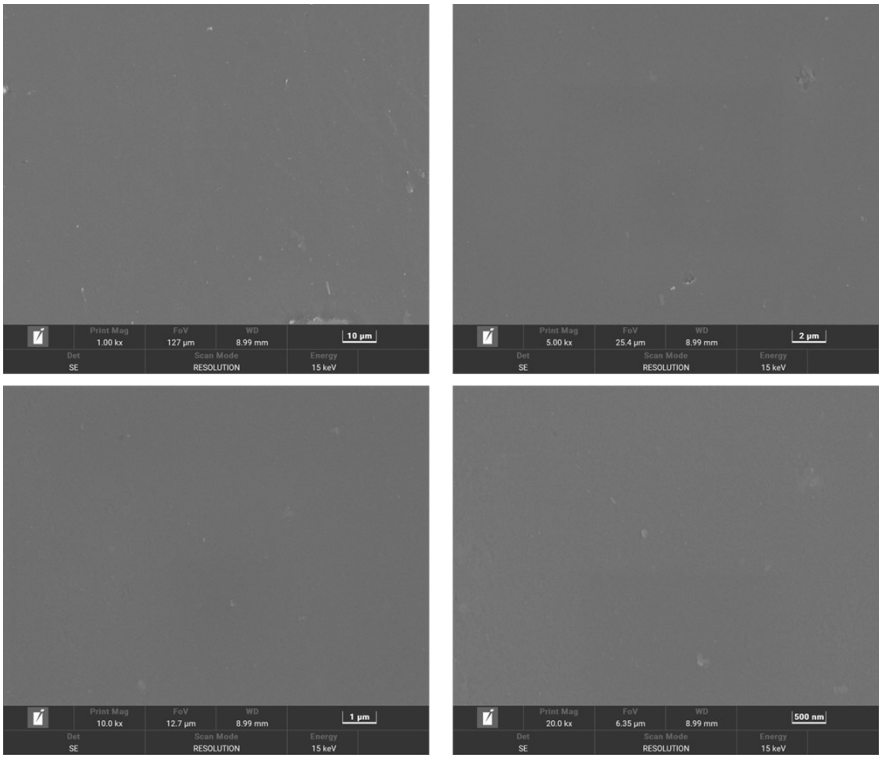

Figure S2. SEM images of **AG**.

4. Powder X-ray diffraction (PXRD) patterns of AG

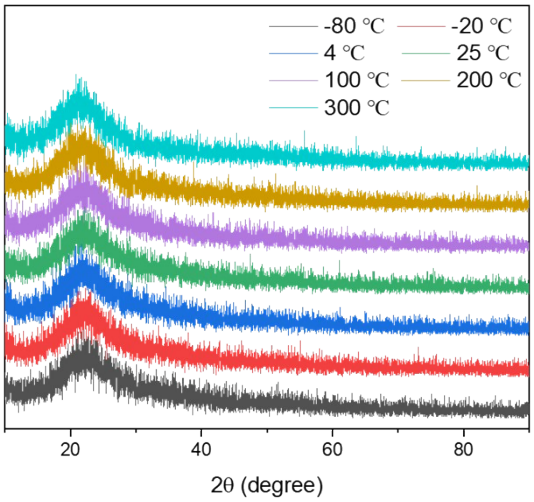

Figure S3. Temperature-dependent PXRD spectra of **AG**.

5. Small angle X-ray scattering (SAXS) of AG

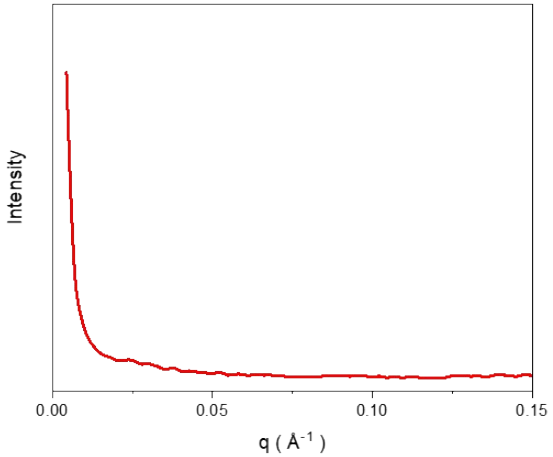

Figure S4. SAXS spectrum of **AG**.

6. Scanning electron microscope (SEM)-Mapping of AG

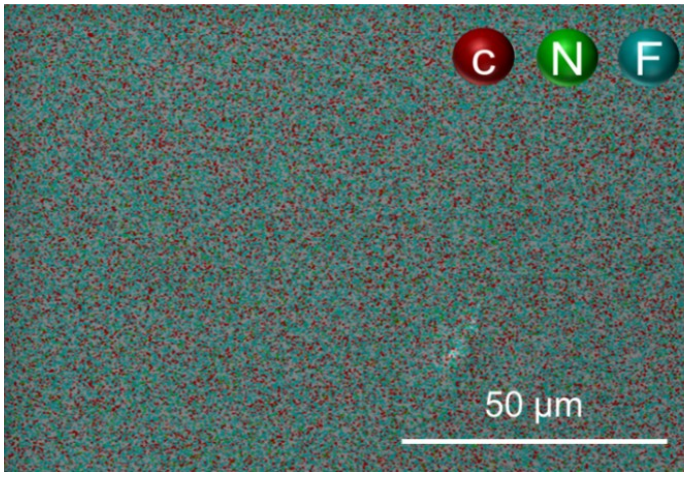

Figure S5.SEM-Mapping image of **AG**.

7. Broadband dielectric measurements of AG

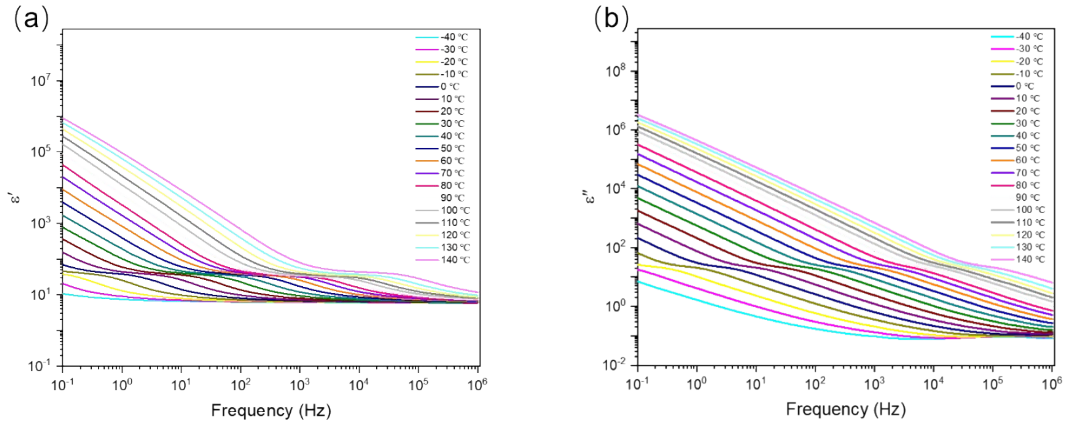

Figure S6. Plots of dielectric constant real part (ε′) and Imaginary part (ε″) as a function of frequency for **AG** from –40 to 140 °C.

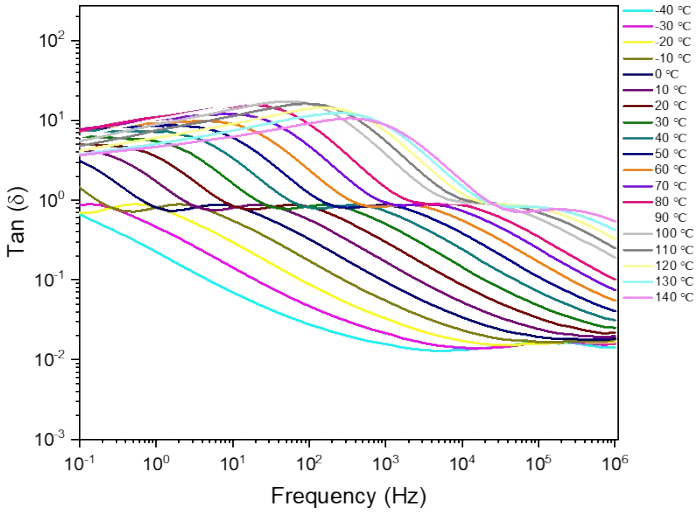

Figure S7. Dielectric loss as a function of frequency for **AG** from –40 to 140 °C.

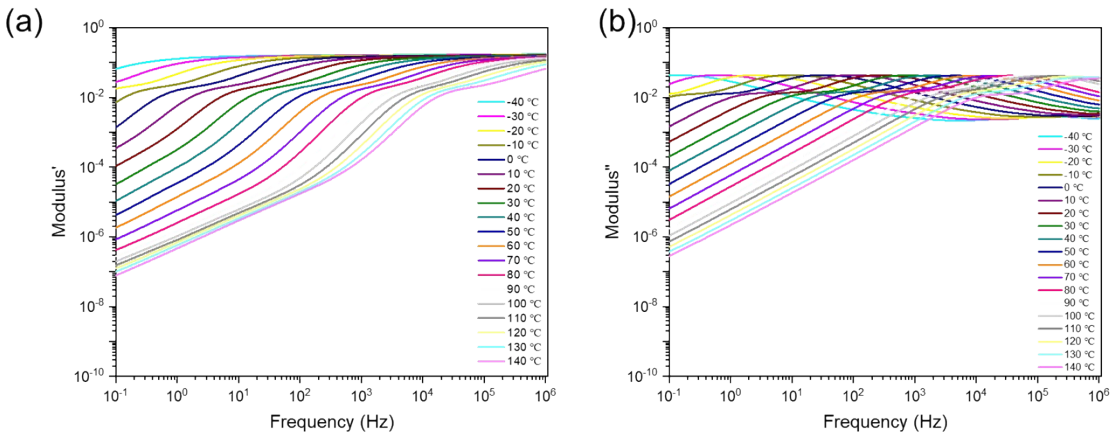

Figure S8. Dielectric modulus' (a) and modulus" (b) as a function of frequency for **AG** from –40 to 140 °C.

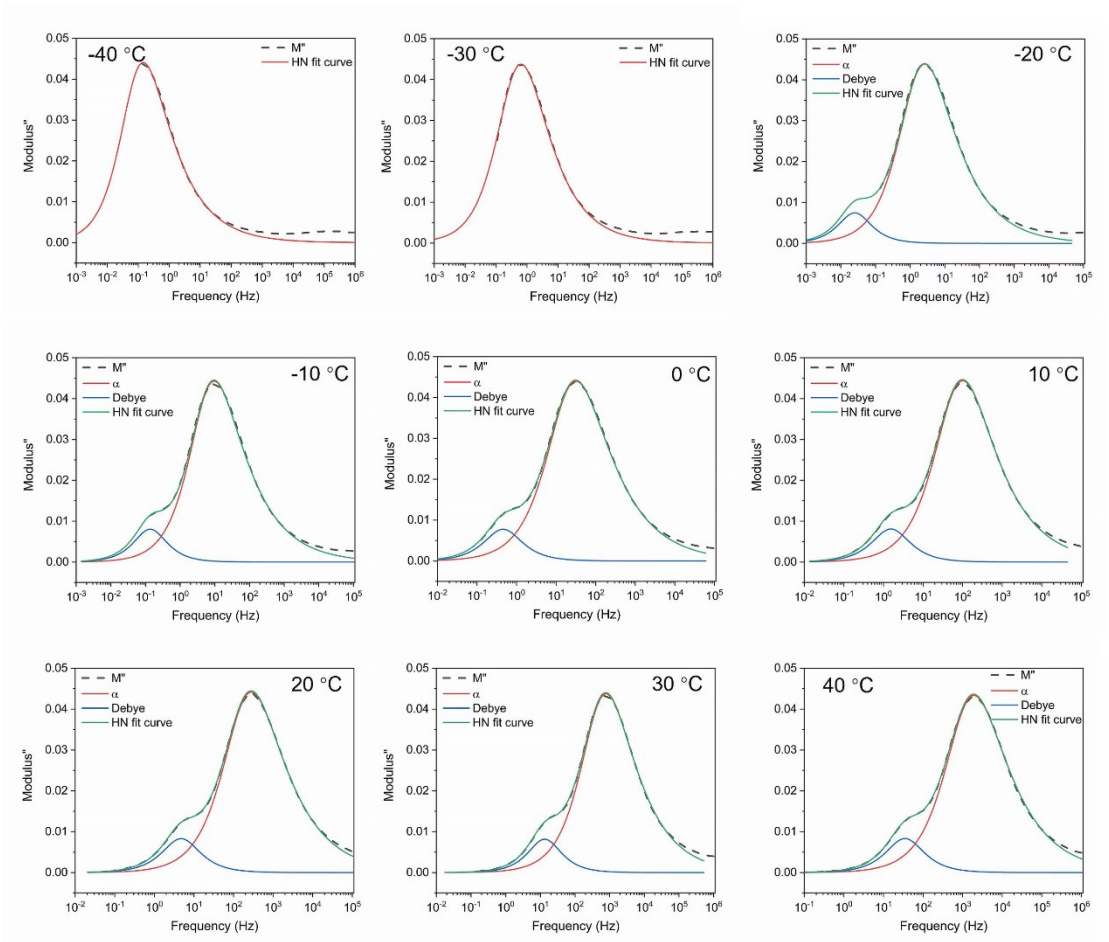
-40 °C
-30 °C
-20 °C
-10 °C
0 °C
10 °C
20 °C
30 °C
40 °C
M"
α
Debye
HN fit curve
Modulus"
Frequency (Hz)

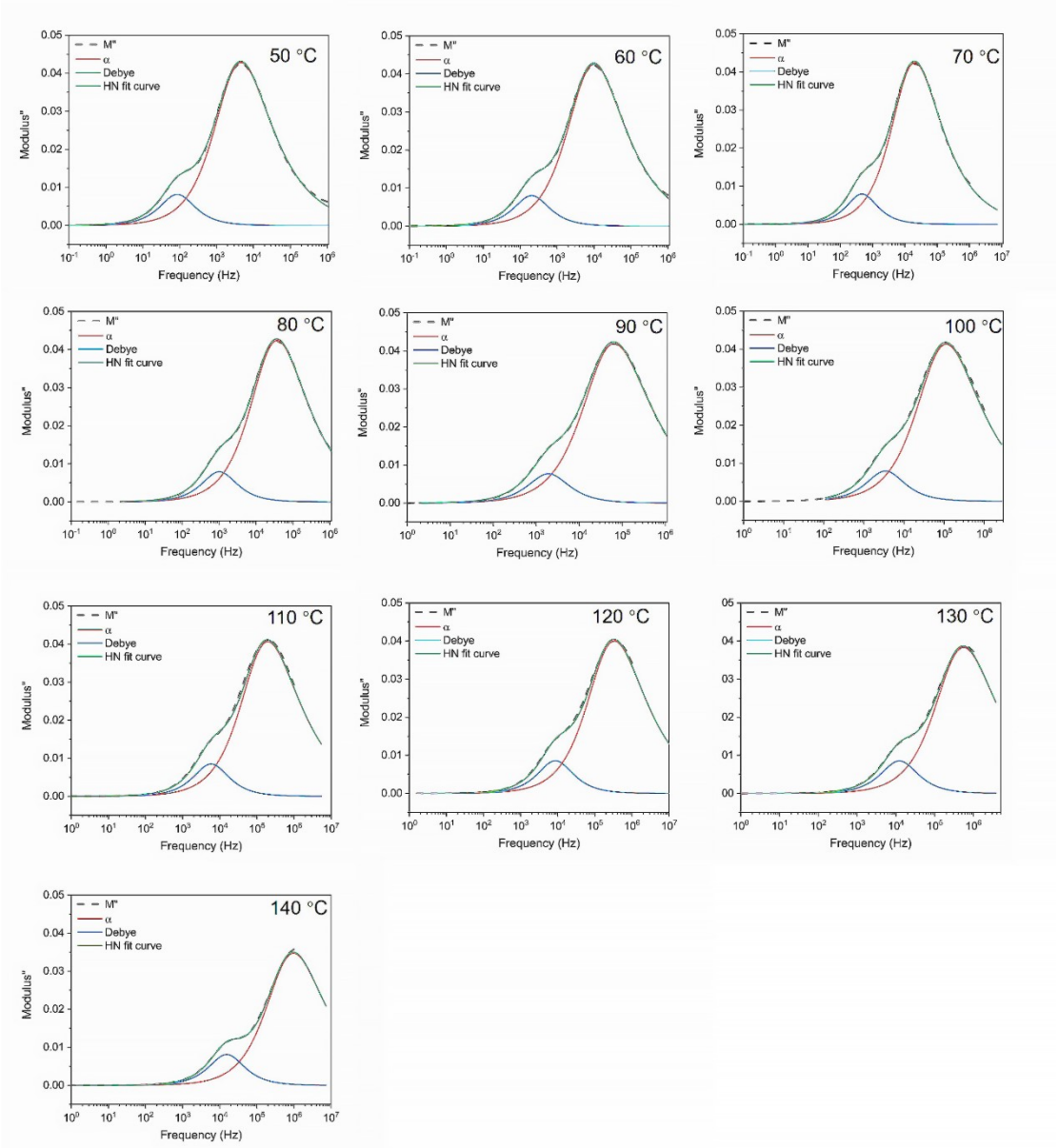

Figure S9 Dielectric modulus" of **AG** fitted by a combination of three Havriliak-Negami (HN) equations from -40 °C to 140 °C.

8. Differential scanning calorimeter (DSC) of AG

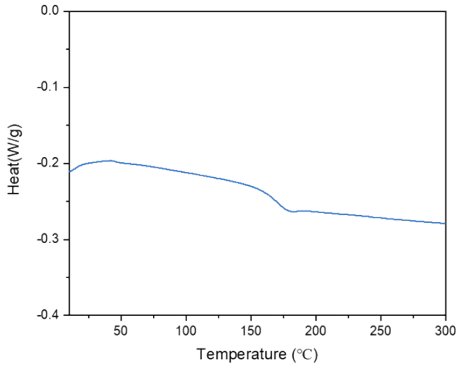

Figure S10. DSC spectrum of **AG**.

9. Simulation calculations

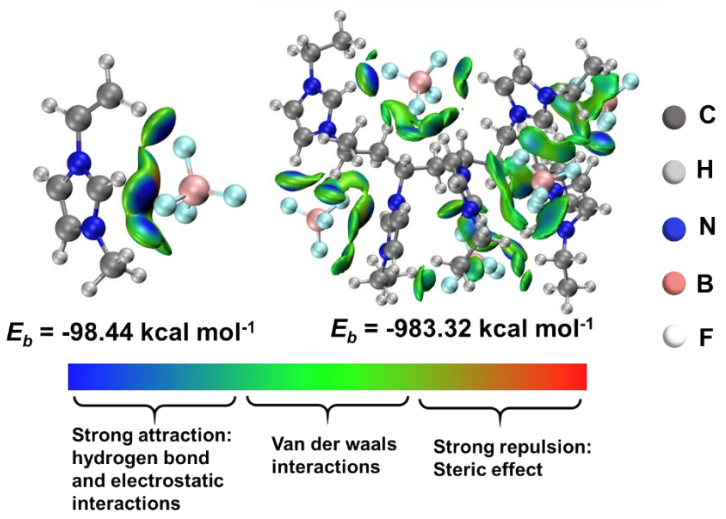

Figure S11. IGM image and Binding energy (E_b) of monomer and **AG**.

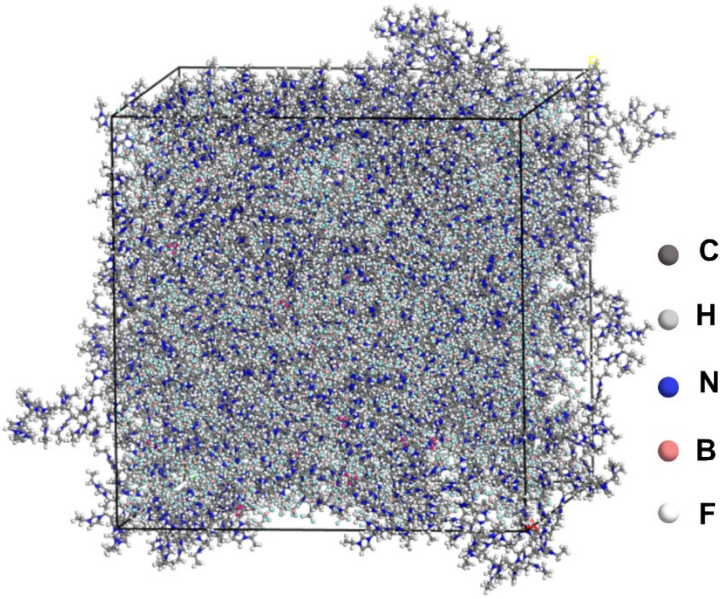

Figure S12. MD model of **AG**.

Table S2. Cohesive energy of **AG**.

Cohesive energy (kJ mol^{-1})	Electrostatic energy (kJ mol^{-1})	Van der Waals (kJ mol^{-1})	Internal potential energy (kJ mol^{-1})
-3.55×10^5	-5.19×10^5	-8.72×10^4	2.51×10^5

10. Solid-phase ultraviolet spectrum of AG

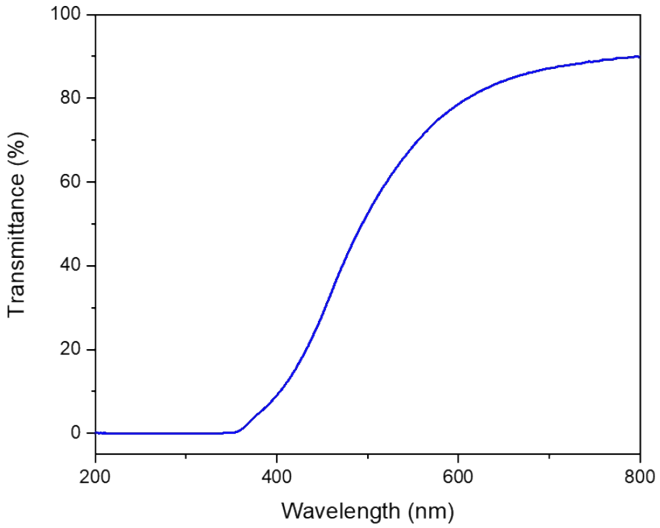

Figure S13. Solid-phase ultraviolet spectrum of **AG**.

11. Fluorescence spectra of monomer and AG

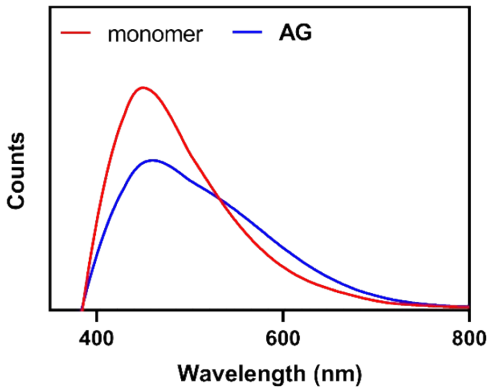

Figure S14. Fluorescence spectra of monomer and **AG** with the E_x at 365 nm.

The quantum yields of monomer and **AG** are 4.23% and 0.74%, respectively.

12. Fracture micrograph of AG

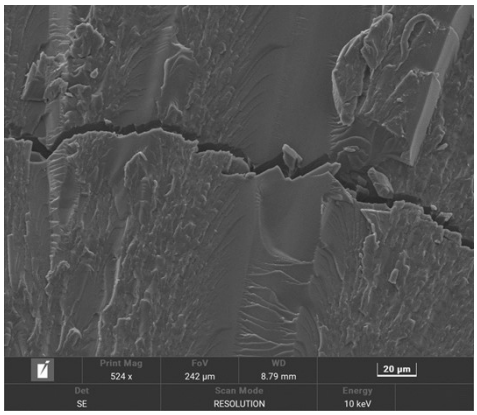

Figure S15. SEM image of the fracture in **AG**.

13. Solvent resistance of AG

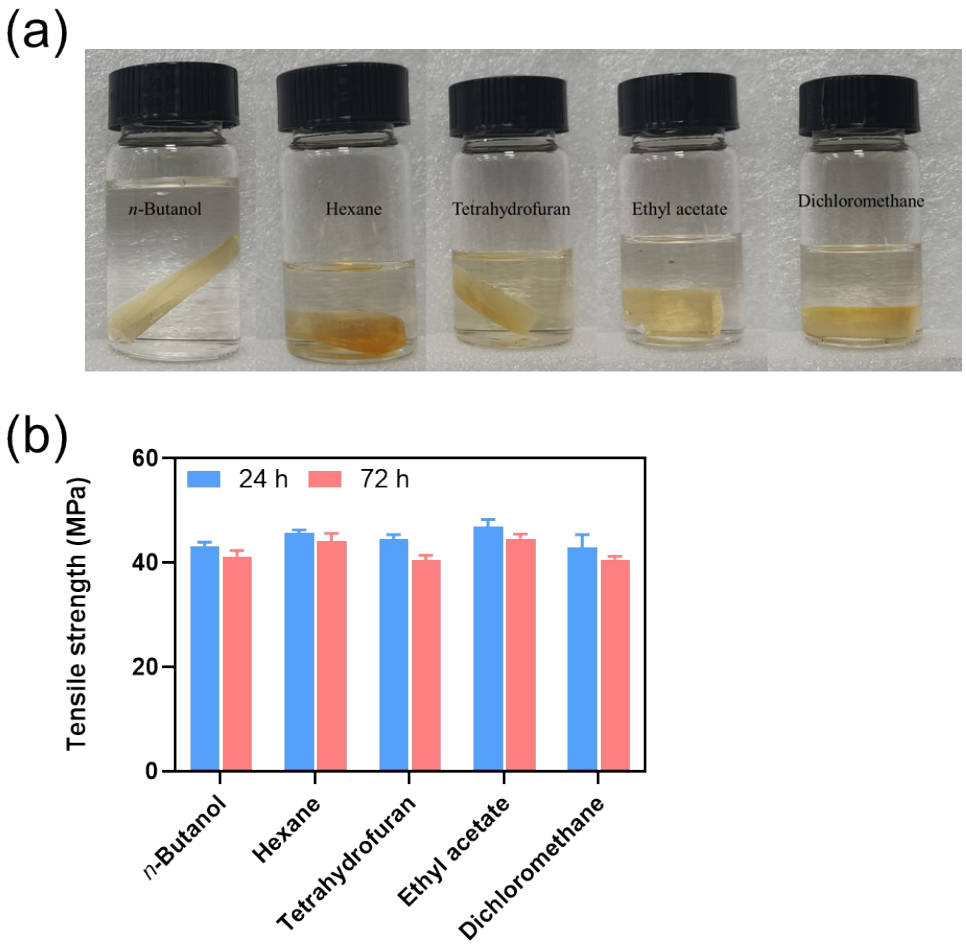

Figure S16. Solvent resistance of **AG**. (a) The photo of **AG** samples immersed in organic solvent for 72 h. (b) The tensile strength of **AG** samples immersed in organic solvent for 24 and 72 h.

14. Dynamic mechanic thermal analysis (DMA) of AG

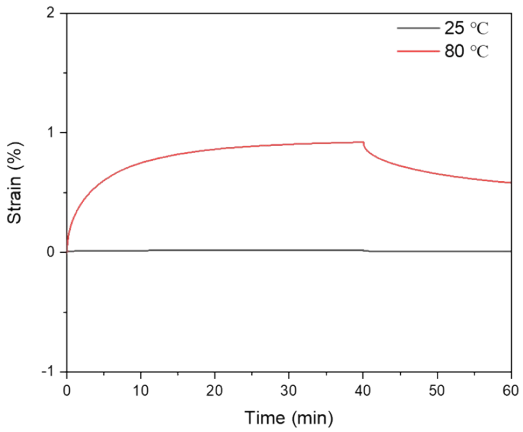

Figure S17. Creep-recovery plots of **AG** at different temperatures. The samples were applied with a constant stress of 0.1 MPa.

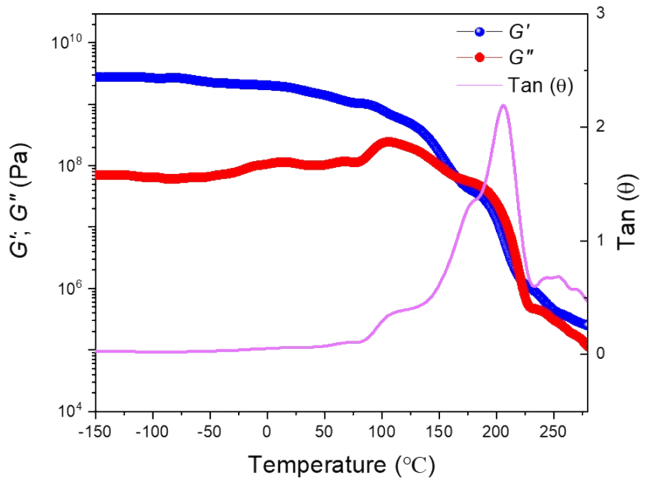

Figure S18. Temperature-dependent of storage modulus (*G'*), loss modulus (*G''*) and loss angle of **AG**.

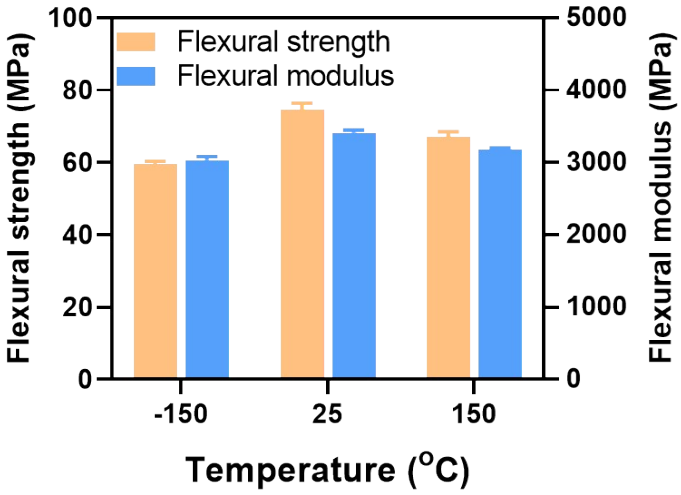

Figure S19. Flexural strength and modulus of **AG** at different temperatures.

15. Flame Retardancy of AG

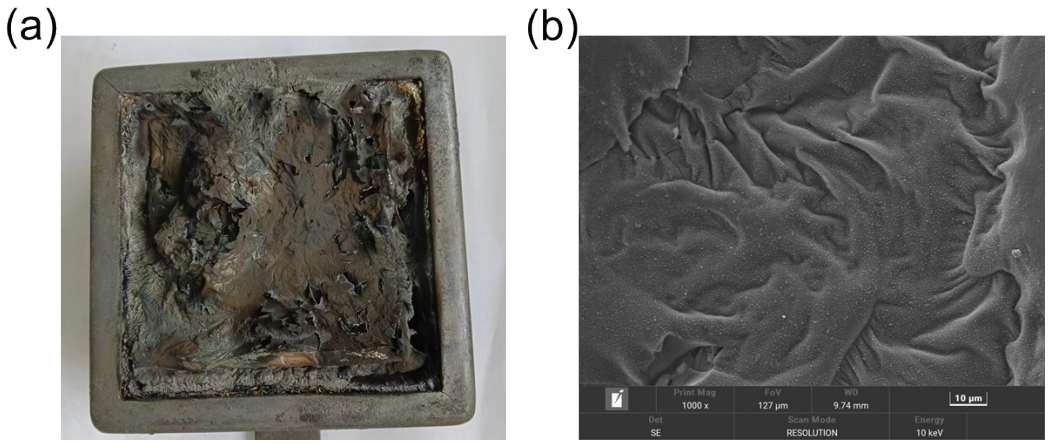

Figure S20. Digital photograph (a) and SEM image (b) of residual chars after cone calorimeter.

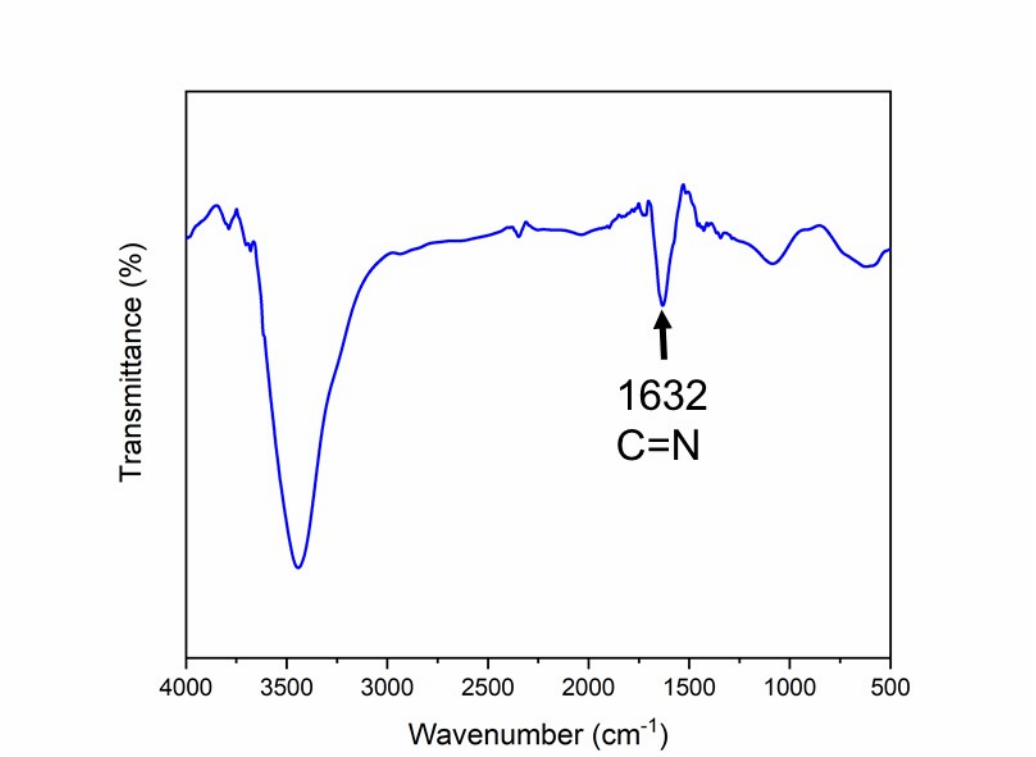

Figure S21. FT-IR spectrum of residual chars after cone calorimeter.

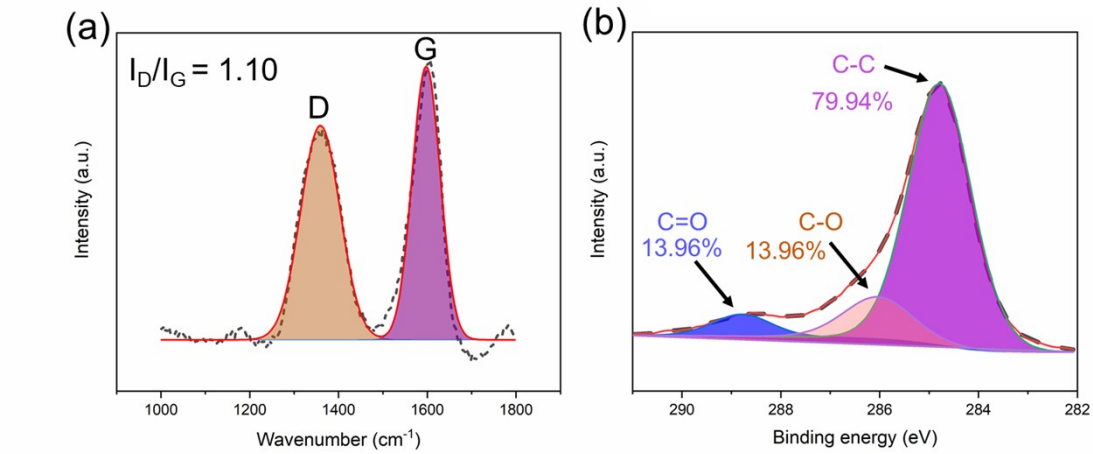

Figure S22. Raman spectroscopic analysis (a) and C1s XPS spectra (b) of residual chars after cone calorimeter.

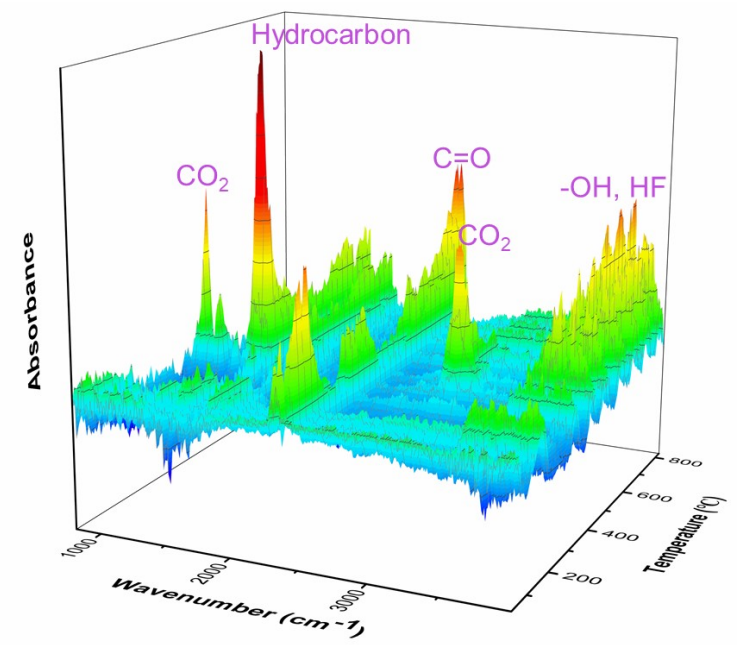

Figure S23. The three-dimensional TG-IR spectra of **AG**.

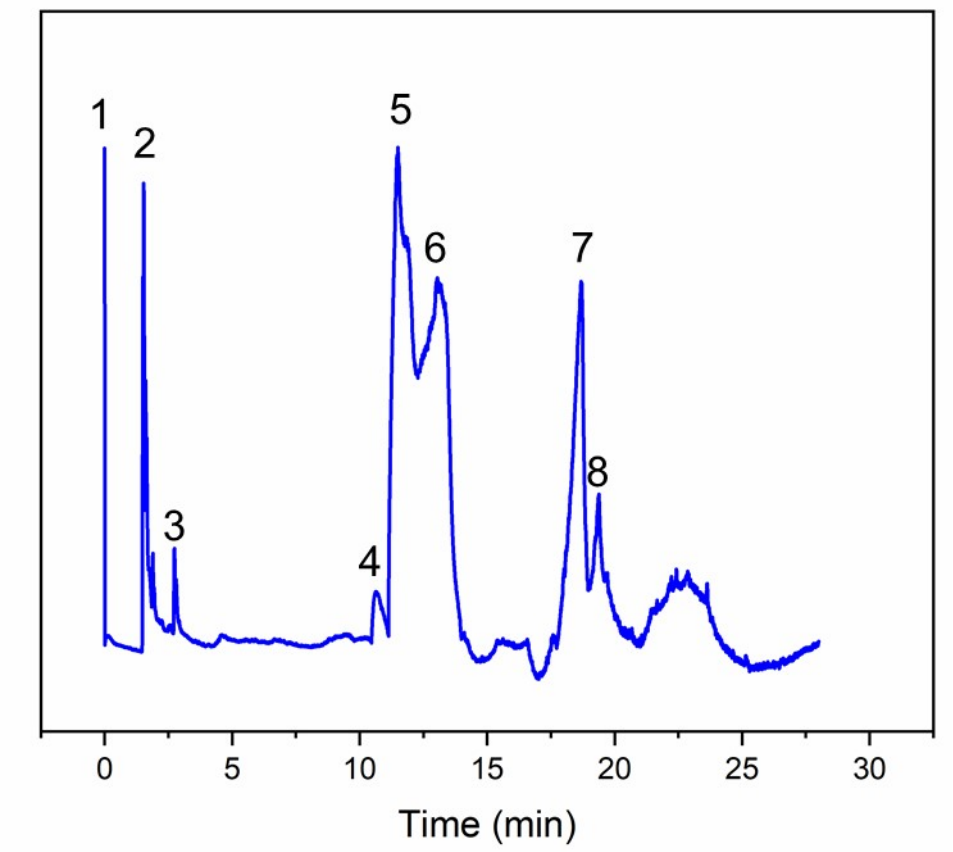

Figure S24. PyGC-MS spectrum (600 °C) of **AG** (1: Nitrous oxide; 2: Ethane; 3: Benzene; 4: N-Vinylimidazole; 5-7: 1-Ethyl-1H-imidazole; 8: N,N-Dimethyl-4-nitrosoaniline; Benzene originates from initiators).

16. Plots of dielectric constant and dielectric loss of AG

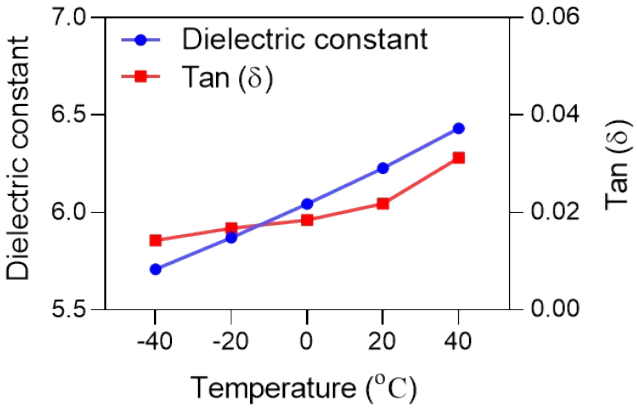

Figure S25. Plots of dielectric constant and dielectric loss of **AG** versus input frequency at different temperatures in a range of −40 to 40 °C.

17. Rebound rates of AG and commercial polymers

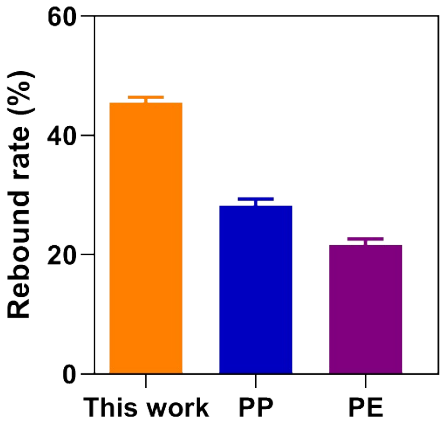

Figure S26. Rebound rates of **AG** and commercial polymers.

18. Comparisons between AG and PMMA or PC

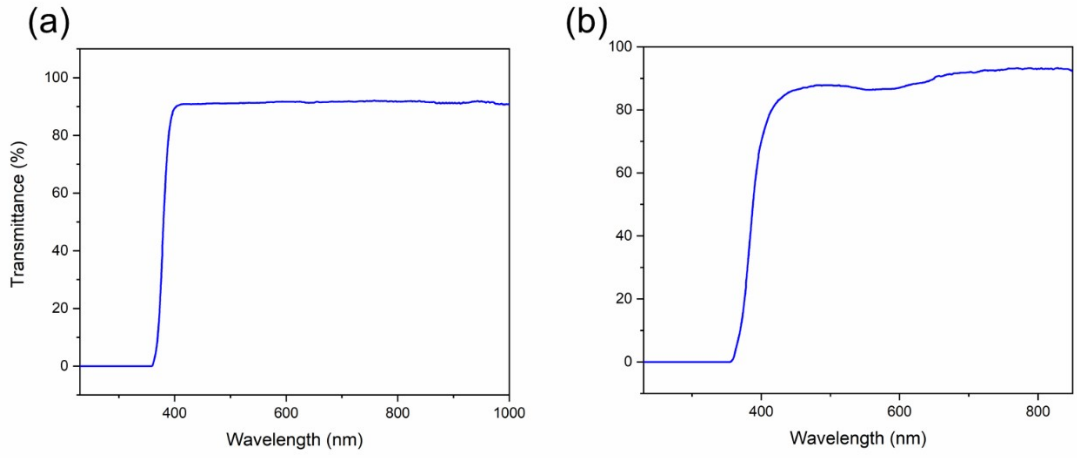

Figure S27. Transmittance of PMMA (a) and PC (b).

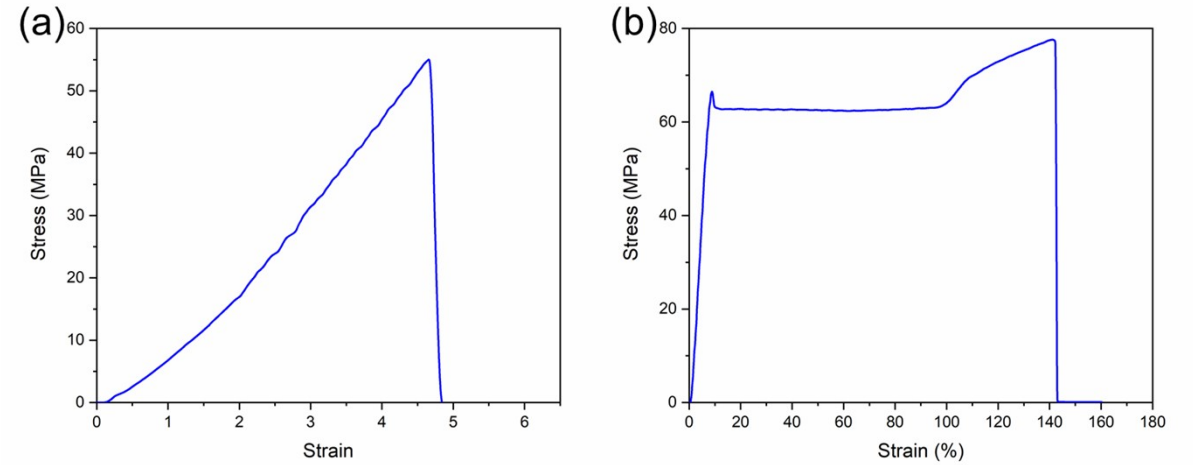

Figure S28. Strain-stress curves of PMMA (a) and PC (b).

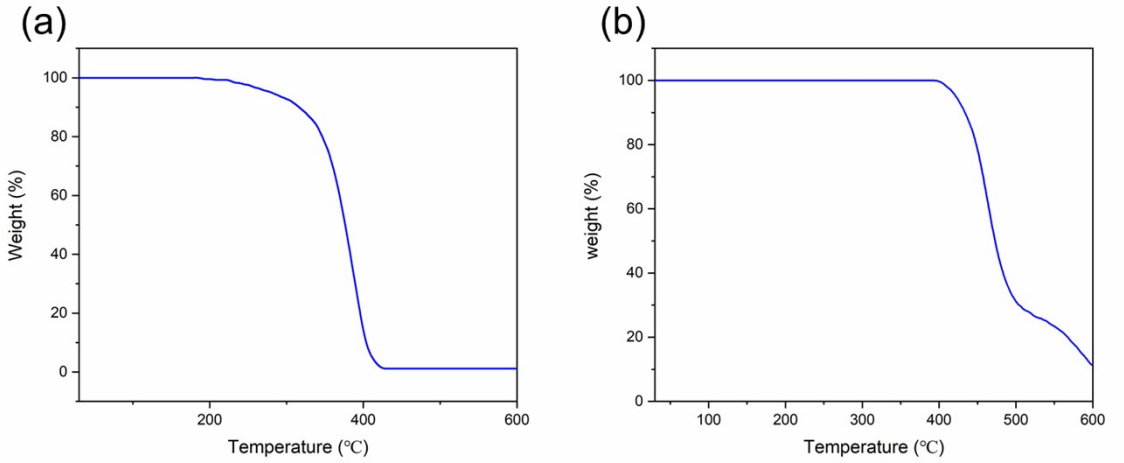

Figure S29. TGA spectra of PMMA (a) and PC (b).

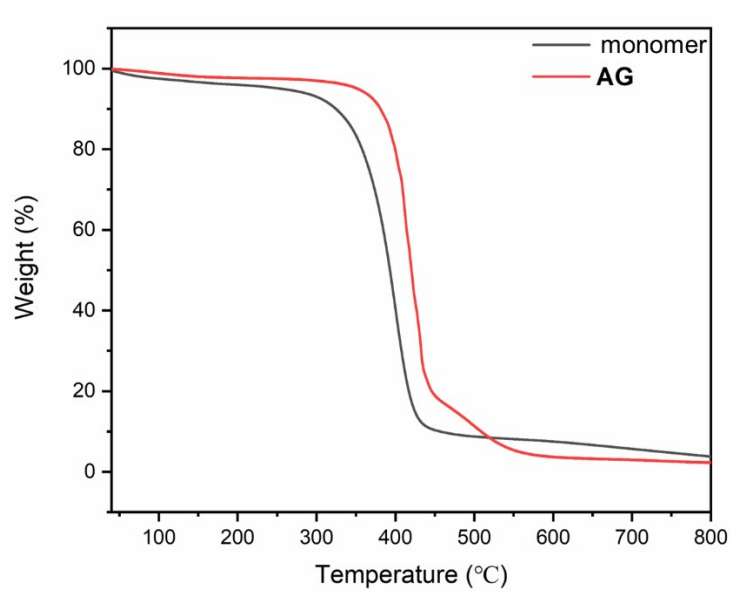

Figure S30. TGA spectra of monomer and **AG**.

Table S3 Comparisons between **AG** and **PMMA** or **PC**.[5,12]

properties	AG	PC	PMMA
Flexural strength (MPa)	74.53	97.27	86.02
Shore hardness (150 °C) (HD)	73.00	40.00	0
Tensile strength (25 °C) (MPa)	61.31	77.58	55.34
Tensile strength (150 °C) (MPa)	48.5	39.51	0
Impact energy (kJ m^{-2})	18.34	163.41	10.11
Flexural modulus (GPa)	3.45	2.41	2.60
Transmittance (%) at 800 nm	90.30	93.10	91.70
Refractive indice	1.47	1.60	1.49
LOI (%)	30.20	24.50	17.30
PHRR (kW m^{-2})	120.80	553	1220
THR (MJ m^{-2})	13.61	78.50	136
TTI (s)	60	56	25
Flame Rating	V-0	V-2	No Rating
Density (g m^{-3})	1.21	1.21	1.19

19. Videos

Video S1. **AG** pressed by a car.
Video S2. Flame retardant test of **AG**.
Video S4. **AG** as the touch screen of mobile phone.
Video S4. **AG** for mobile phone protection.

20. References

1 L. Xu, Z. Huang, Z. Deng, Z. Du, T. L. Sun, Z.-H. Guo, K. Yue, *Adv. Mater.* 2021, **33**, 2105306.

2 L. Song, Y. Gao, P. Zou, W. Xu, M. Gao, Y. Zhang, J. Huo, F. Li, J. Qiao, L.-M. Wang, J.-Q. Wang, *P. Natl. Acad. Sci. USA* 2023, **120**, e2302776120.

3 N. Kaur, M. Singh, L. Singh, A. M. Awasthi, S. P. Lochab, *Mater. Res. Bull.* 2015, **63**, 24–31.

4 J. Chen, Y. Ma, T. Chen, Y. Du, J. Xu, D. Wang, J. Yang, P. Hu, J. Jing, B. Yao, J. Fu, *Adv. Funct. Mater.* 2023, **33**, 2212564.

5 Z. Liu, M. Ma, B. Ge, Y. Zheng, S. Chen, Y. Shi, H. He, Y. Zhu, X. Wang, *Chem. Eng. J.* 2023, **474**, 145799.

6 C. Lefebvre, G. Rubez, H. Khartabil, J.-C. Boisson, J. Contreras-García, E. Hénon, *Phys.*

Chem. Chem. Phys. 2017, **19**, 17928–17936.

7 T. Lu, F. Chen, *J. Comput. Chem.* 2012, **33**, 580–592.

8 X. Tan, X. Liu, X. Yao, Y. Zhang, K. Jiang, *Ind. Eng. Chem. Res*. 2019, **58**, 34–43.

9 J. Wang, R. M. Wolf, J. W. Caldwell, P. A. Kollman, D. A. *J. Comput. Chem*. 2004, **25**, 1157–1174.

10 L. Martínez, R. Andrade, E. G. Birgin, J. M. Martínez, *J. Comput. Chem.* 2009, **30**, 2157–2164.

11 Z. Xie, S. Liu, L. Qin, S. Pang, W. Wang, Y., L. Yan Yao, Z. Chen, S. Wang, H. Du, M. Yu, G. G. Qin, *Opt. Mater. Express* 2015, **5**, 29–43.

12 C. Yi, C. Xu, N. Sun, J. Xu, M. Ma, Y. Shi, H. He, S. Chen, X. Wang, *ACS Appl. Polym. Mater.* 2023, **5**, 846–855.